EUROPEAN JOURNAL OF MECHANICS - B/FLUIDS

[AN OFFICIAL MEDIUM OF PUBLICATION FOR EUROMECH EUROPEAN MECHANICS SOCIETY]

Impact Factor: 2.098

Publisher: Elsevier

Accepted March 29th 2018

THREE-LAYERED ELECTRO-OSMOSIS MODULATED BLOOD FLOW THROUGH A MICRO-CHANNEL

[#1]Dharmendra Tripathi, [1]Ravinder Jhorar, [1]Abhilesh Borode *and* [2]O. Anwar Bég

[1]Department of Mechanical Engineering, Manipal University Jaipur, Rajasthan--303007, India.
[2]Department of Mechanical and Aeronautical Engineering, Salford University, Salford, M54WT, UK.
[#]Corresponding author- email: dharmtri@gmail.com

ABSTRACT

Electrokinetic peristaltic multi-layered transport is considered in a micro-channel under the action of an axial electrical field. Three different layers i.e. the *core layer, intermediate layer and peripheral layer* are simulated with three different viscosities for each fluid layer. The unsteady two-dimensional conservation equations for mass and momentum with electrokinetic body forces, are transformed from the wave frame to the laboratory frame and the electrical field terms are rendered into electrical potential terms via the Poisson-Boltzmann equation, Debye length approximation and ionic Nernst Planck equation. The dimensionless emerging linearized electrokinetic boundary value problem is solved using integral methods. Closed-form expressions are derived for stream functions in the core, intermediate and peripheral layers. Expressions are also derived for the core-intermediate interface shape and the intermediate-peripheral interface shape. Maximum pressures are also computed. To study bolus migration, the range of the trapping limit is also determined in the peripheral layer. It is found that in the core layer larger boluses are computed in the case of lower intermediate layer viscosity relative to peripheral layer viscosity although the number of boluses is greater when the intermediate layer viscosity exceeds the peripheral layer viscosity. Furthermore, in the intermediate layer, stronger concentration of streamlines is computed in the lower half space with positive Helmholtz-Smoluchowski velocity. Also, negative Helmholtz-Smoluchowski velocity reduces the core layer (H_1) interface shape whereas it enhances the peripheral layer *(H)* and intermediate layer (H_2) shapes. At lower values of volume flow rate ratio, hydromechanical efficiency is *maximum for* positive Helmholtz-Smoluchowski velocity whether intermediate layer viscosity is less or greater than peripheral layer viscosity. Finally, greater with greater peristaltic wave amplitude and also for positive Helmholtz-Smoluchowski velocity there is an increase in time-averaged flow rate, whether intermediate layer viscosity is less or greater than peripheral layer viscosity. The analysis is relevant to electro-kinetic hemodynamics and bio-micro-fluidics.

KEYWORDS: *Electrokinetics; blood flow; multi-layered microchannel; thin electric double layer; fluid-fluid interfaces; trapping; bio-micro-fluidics.*

I. INTRODUCTION

Electro-osmotic blood flow arises frequently in capillaries and other narrow vessels. Blood contains many constituents including ions and the bio-electric field generates electrical Coulomb forces which act on these ions [1]. When subjected to an external electrical field, blood flow can be further controlled via electro-osmotic processes [2]. Electrokinetic motion of the particles embodies the migration of electrically charged or uncharged particles in an aqueous solution or suspension, in the presence of an applied electric field. Electrokinetic phenomena embody many different effects including electrophoresis, diffusiophoresis, electro-osmosis and capillary osmosis. This branch of fluid mechanics has attracted significant attention in recent years with developments in medical engineering at progressively smaller length scales i.e. micro- and nano-scales. Both experimental and computational investigations have been reported. Examples of recent studies of electrokinetic flows include biomicrofluidic mixers which amalgamate alternating electrical excitation with pressure-driven base electro-osmotic flow in complex microchannel geometries. Xing et al. [4] investigated the use of electro-osmotics in plasmapheresis devices with thermal effects (Joule heating). Pikal [5] has considered electrokinetic flows in transdermal iontophoresis [5]. Analytical investigations have of electro-osmotic flows have also been reported. Levine et al. [6] provided one of the earliest theoretical studies of electrokinetic flow and showed that the electro-viscous retardation effect achieves a maximum impact both with regard to electrokinetic radius and also with respect to zeta-potential. Ghosal [7] investigated analytically the influence of axial cross-section on electrokinetic flow in micro-channels, noting that an induced pressure gradient arises with an associated secondary flow which enhances Taylor dispersion. Misra et al. [8] investigated theoretically the electroosmotic micropolar flow in a vibrating microchannel, solving the coupled linear and angular momentum and Gauss charge conservation equations under the Debye-Hückel approximation. Jubery [9] conducted numerical simulations of electrokinetic effects on blood flows using a distributed Lagrange multiplier multi-domain method for electric potential. This study also addressed in detail the dielectrophoretic separation of particles [10]. Dutta et al. [11] used a spectral element method to simulate mixed electroosmotic/pressure driven flows in a T-junction under various external electric field strengths.

Novel developments in pumping techniques in micro-systems have also embraced electrokinetic mechanisms. Interesting studies in this regard include Fu et al. [12] who have studied applications

in ctyometry. Wong et al. [13] have reviewed alternating current (AC) electrokinetics for manipulating bulk fluid mass and embedded in clinical diagnostics. Further studies include Jie et al. [14] on electrothermal micropumping of medicines and Park et al. [15] on dielectrophoretic bacterial separation technologies. Electrokinetic micro-pumping fabrication has been addressed by Kang et al. [16]. Other intriguing applications of electro-kinetics include AC electro-osmotic (ACEO) pumping [17], travelling-wave electroosmosis (TWEO) pulsed microfluidics [18] and mechanical actuation devices [19].

Peristalsis is a complex and efficient biological propulsion mechanism arising in gastro-intestinal movement, blood flow, worm dynamics and plant trans-location. Peristalsis is a radially symmetrical contraction and relaxation of muscles which serves to effectively pump fluids in a wave-like motion along a conduit utilizing deformable walls. In the human digestive system it is induced by reflexes in the enteric nervous systems which are generated by physical movement of a bolus (foodstuff). Peristaltic fluid dynamics has been lucidly reviewed by Fung [19]. It has also received substantial interest in the engineering sciences community. Representative studies of peristaltic propulsion in biological vessels include Whirlow et al. [21] who considered pumping of Newtonian viscous fluids in thick-walled deformable tubes. Grabski et al. [22] conducted a computational analysis of peristaltic flow of Newtonian fluid in two-dimensional channel using a high-order iterative formulation and radial basis functions for both vanishing and finite Reynolds numbers. Khabazi et al. [23] investigated peristaltic transport of a Bingham viscoplastic fluid in a planar two-dimensional channel with the multiple-relaxation-time lattice Boltzmann method (MRT-LBM). They observed that a threshold wave number exists above which the yield stress of the fluid may accelerate flow whereas below this threshold a deceleration is induced. Javed et al. [24] derived closed-form solutions for peristaltic flow and heat transfer of a Walters-B viscoelastic fluid in a compliant wall channel. Tripathi and Bég [25] investigated magnetic field and wave amplitude effects on transient magnetohydrodynamic peristaltic heat transfer in finite length channel. Peristaltic electrokinetic blood flow in cylindrical finite length capillaries was studied very recently by Tripathi et al. [26] who observed that increasing axial electrical field enhances pressure whereas it reduces bolus size. They also computed that with greater electro-osmotic parameter (smaller Debye length) volumetric flow rate is increased whereas it is lowered with stronger Helmholtz–Smoluchowski velocity (greater external axial electric field).

In various physiological flows including chyme transport in the small intestines and small blood vessels, viscosity variation is known to occur. In capillaries, the viscosity of the peripheral layer is usually less than that of the core layer. The thinner peripheral layer results in an enhanced volumetric flow-rate. Furthermore in micro-peristaltic pumps, a peripheral layer can be instrumental in avoiding contact of toxic fluids with mechanical components which could result in corrosion and contamination. These applications require multi-layered viscous peristaltic transport models. Important works in this regard include Shukla et al. [26] who considered a two-layered peristaltic model and identified that that the interface shape is influenced by the viscosity ratio of the fluids in the two (central and peripheral) layers rather than the geometric ratio of the radii of the outer (peripheral) and the central layers. Further investigations have been reported by Srivastava and Srivastava [28] who presented a two-fluid (peripheral and core fluid) model for a non-uniform tube and channel has been investigated under the lubrication approximation, noting that flow rate is elevated as the viscosity of the peripheral layer fluid is reduced. Srivastava and Saxena [29] examined peristaltic two-fluid blood flow comprising a core region of suspension of all the erythrocytes, assumed to be a Casson fluid, and a peripheral layer of plasma (Newtonian fluid). Elshehawey and Gharsseldien [30] studied peristaltic pumping of three-layered flow with variable viscosity for an incompressible Newtonian fluid through a channel. They showed that interfacial shapes, flow rates and hydromechanical efficiency are more significantly modified by viscosity variation in the peripheral layer compared with the intermediate layer. Pandey et al. [31] considered two-dimensional peristaltic flow of power-law fluids in three layers with different viscosities, noting that flow rate is elevated with the viscosities of the peripheral and the intermediate layers whereas a more impactful influence is computed with the viscosity of the outermost layer. Misra and Pandey [32] also analyzed peristaltic pumping of a power-law fluid in a cylindrical tube in the presence of a peripheral layer of another power-law fluid with different viscosity, observing that flow-rate is reduced with decreasing flow behaviour index or outer layer viscosity.

An inspection of the literature reveals that there is an absence of studies of electrokinetic peristaltic flows in multi-layered viscous fluids. This is the objective of the present study. Although interfacial electrokinetic flows have been investigated by Berry et al. [33], their study did not consider peristalsis. Multi-layered viscous peristaltic flows may find important applications in further elucidating electro-osmotic blood flows in more realistic hemodynamic scenarios [34].

They may also have relevance to more elaborate micro-peristaltic pump devices. Combined study of electroosmotic flow via peristaltic pumping was firstly reported by Chakraborty [35] who discussed the alteration of peristaltic flow through electroosmotic mechanism. This model is further extended by Misra et al. [36] for micropolar fluids, Bandopadhyay et al. [37] for electric double layer phenomenon, Tripathi et al. [38] for electromagnetohydrodynamics (EMHD), Tripathi et al. [39] for viscoelastic physiological fluids and Tripathi et al. [40] for capillary hemodynamics through electroosmosis mechanisms. All extended works reported only single layer electroosmotic flow via peristaltic pumping. Considering the multilayered flow which is more applicable in blood flow, Goswami et al. [41] have presented a mathematical model to study the electrokinetically modulated two layered flow of power law fluids. A thin electric double layer (EDL) approximation is adopted where only electroosmotic velocity is taken as slip velocity at the surface of peripheral layer. Still there is a gap to investigate electroosmosis modulated three layered flow via peristaltic pumping. In the present study we consider a three-layered model for electro-osmotic peristaltic pumping. Closed-form solutions are presented for the transformed boundary value problem. The effects of intermediate and peripheral layer viscosities and Helmholtz-Smoluchowski (maximum electro-osmotic) velocity on interface shapes, pressure rise, mechanical efficiency and maximum time averaged flow rate are computed. The influence of wave amplitude and Helmholtz-Smoluchowski velocity on streamline distributions in the intermediate layer and peripheral layer are also visualized and bolus dynamics examinecd carefully.

2. MATHEMATICAL MODEL

We analyze three layered flow in (core layer, intermediate layer, and peripheral layer) of viscous fluids (blood) of different viscosity (μ_0, μ_1, μ_2) respectively through micro-channel. The schematic of the problem under consideration is depicted in **Fig. 1,** under axial electric field. We consider a sinusoidal wall surface propagating with wave velocity (c) and wavelength (λ). The peripheral wall surface is taken negatively charged and the physiological fluid (blood) is considered as an aqueous ionic solution to study the thin electric double layer (EDL) effects. The mathematical equation for wall surface is expressed as:

$$H(x,t) = a + \phi \sin \frac{2\pi}{\lambda}(x - ct) \ , \tag{1}$$

where $a, \phi, \lambda, x, c, t$ are the radius of tube, amplitude of the wave, wavelength, axial coordinate, wave velocity, and time. The governing equation for unsteady momentum conservation in the axial direction for axisymmetric incompressible peristaltic flow with an axially applied electrokinetic body force term taken into account, takes the form [30, 41]:

$$\rho\left[\frac{\partial u}{\partial t}+u\frac{\partial u}{\partial x}+v\frac{\partial u}{\partial y}\right]=-\frac{\partial P}{\partial x}+2\frac{\partial}{\partial x}\left[\mu\frac{\partial u}{\partial x}\right]+\frac{\partial}{\partial y}\left[\mu\left(\frac{\partial u}{\partial y}+\frac{\partial v}{\partial x}\right)\right]+\rho_e E_x\,, \tag{2}$$

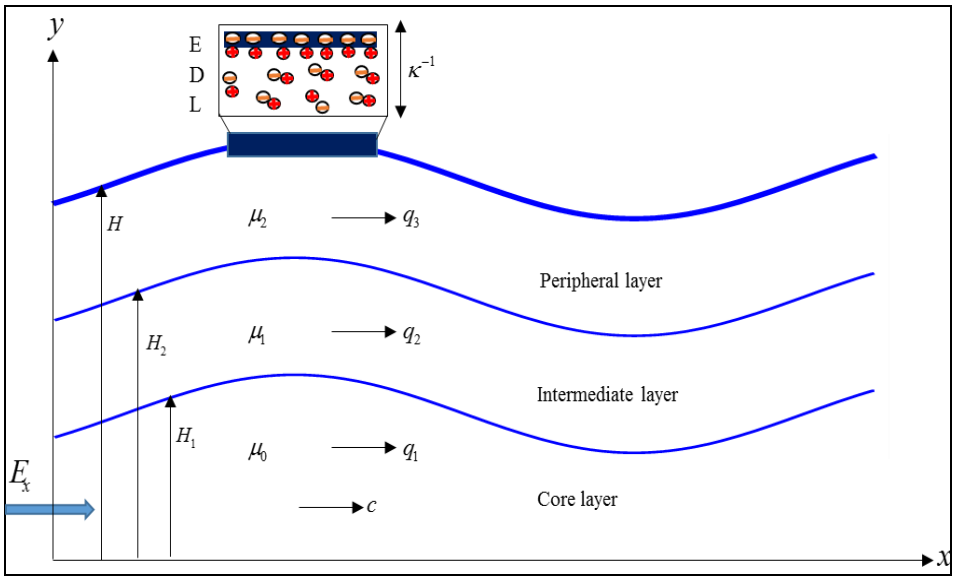

Figure 1: A geometrical description of three-layered blood flow through a microchannel augmented by external electric field with thin EDL formation.

where $\rho, u, p,$ and E_x denote the fluid density, axial velocity, pressure, and external electric field, respectively and μ is the variable viscosity considered as:

$$\mu=\begin{cases}\mu_0, & 0\le y\le H_1,\\ \mu_1, & H_1\le y\le H_2\,,\\ \mu_2, & H_2\le y\le H\,.\end{cases} \tag{3}$$

We have considered a negatively charged surface (microchannel wall) and aqueous (polar) solvent in this model. For a symmetric binary electrolyte solution (Na^+ Cl^-), the electric potential distribution is developed due to the presence of electrical double layer (EDL) in the microchannel, described by the Poisson equation:

$$\nabla^2\Phi = -\frac{\rho_e}{\varepsilon}, \tag{4}$$

in which, ∇^2 is Laplacian operator, Φ is electrical potential function, ρ_e is the density of the total ionic charge, ε is the permittivity. For a symmetric electrolyte, the density of the total ionic energy, ρ_e is given by, $\rho_e = ez(n^+ - n^-)$, in which z is charge balance, e is the electronic charge, n^+ and n^- are the number densities of cations and anions respectively. For this, the ionic number distributions of the individual species are given by the Nernst-Planck equation for each species as:

$$\frac{\partial n_\pm}{\partial t} + u\frac{\partial n_\pm}{\partial x} + v\frac{\partial n_\pm}{\partial y} = D\left(\frac{\partial^2 n_\pm}{\partial x^2} + \frac{\partial^2 n_\pm}{\partial y^2}\right) \pm \frac{Dze}{k_B T}\left(\frac{\partial}{\partial x}\left(n_\pm \frac{\partial \Phi}{\partial x}\right) + \frac{\partial}{\partial y}\left(n_\pm \frac{\partial \Phi}{\partial y}\right)\right). \tag{5}$$

Implicit in this analysis, is the assumption of equal ionic diffusion coefficients for both the species, and that the mobility of the species is given by the Einstein formula where D represents the diffusivity of the chemical species and k_B is Boltzmann constant. The following non-dimensional parameters are defined to simplify the model:

$$\bar{x} = \frac{x}{\lambda},\ \bar{y} = \frac{y}{a},\ \bar{t} = \frac{ct}{\lambda},\ \bar{u} = \frac{u}{c},\ \bar{v} = \frac{v}{c\delta},\ \ \bar{\mu} = \frac{\mu}{\mu_0}, \bar{H}, \bar{H}_1, \bar{H}_2 = \frac{H, H_1, H_2}{a}, \bar{p} = \frac{pa^2}{\lambda c \mu_0},$$

$$\bar{\phi} = \frac{\phi}{a}, \bar{\Phi} = \frac{\Phi}{\zeta}, \bar{n} = \frac{n}{n_0}. \tag{6}$$

Furthermore, the nonlinear terms $O\left(Pe\,\delta^2\right)$, where $Pe = Re\,Sc$ represents the ionic Peclet number, *Re* is Reynolds number and $Sc = \mu_0/\rho D$ denotes the Schmidt number which may be dropped in the limit that *Re, Pe,* δ <<1. Using the above limitations, thin electric double layer limit (κa<<1) approximations and also dropping the bar, the Poisson equation, Nernst Planck equations, and momentum equations reduce to:

$$\frac{\partial^2 \Phi}{\partial y^2} = -\kappa^2\left(\frac{n_+ - n_-}{2}\right), \tag{7}$$

$$0 = \frac{\partial^2 n_\pm}{\partial y^2} \pm \frac{\partial}{\partial y}\left(n_\pm \frac{\partial \Phi}{\partial y}\right), \tag{8}$$

$$\frac{\partial p}{\partial x} = \frac{\partial}{\partial y}\left(\mu \frac{\partial u}{\partial y}\right), \tag{9}$$

where $\kappa = aez\sqrt{\frac{2n_0}{\varepsilon K_B T}} = \frac{a}{\lambda_d}$, is known as the electro-osmotic parameter (reciprocal of Debye length). In this thin Debye layer and weak electric field limit, the description in the inner region follows the conventional analysis of electroosmotic flow problems and results in a "bulk" velocity of ($U_{HS} = -\frac{E_x \varepsilon z}{\mu c}$), which may be used as a boundary condition i.e. $u = U_{HS}$ at the wall of peripheral layer ($y = H$). The transformations between wave frame and laboratory frame are given by: $x_w = x - t$, $y = y$, $u_w = u - 1$, $v = v, q = Q - h$. Imposing the stream function in the wave frame, defined as: $u = \frac{\partial \psi}{\partial y}$ and $v = -\frac{\partial \psi}{\partial x_w}$, Eqn. (9) can be expressed as:

$$\frac{\partial p}{\partial x_w} = \frac{\partial}{\partial y}\left(\mu \frac{\partial^2 \psi}{\partial y^2}\right). \tag{10}$$

The volumetric flow rate in terms of *time-averaged* volumetric flow rate is defined as:

$$q = \bar{Q} - 1 = q_1 + q_2 + q_3, \tag{11a}$$

$$q_1^* = \bar{Q}_1 - \int_0^1 H_1 dx_w = q_1, \tag{11b}$$

$$q_2^* = \bar{Q}_2 - \int_0^1 H_2 dx_w = q_1 + q_2, \tag{11c}$$

where q_1, q_2, q_3 are the volumetric flow rates, in the core, intermediate, and peripheral regions, respectively, in the *wave frame* and $\bar{Q} = \int_0^1 Q dt$ is the total volume flow rate averaged over a period, henceforth known as the *time-averaged flow rate*. The following boundary conditions are imposed:

$$\psi = 0,\ \psi_{yy} = 0 \text{ at } y = 0, \tag{12a}$$

$$\psi_y = U_{HS} - 1 \text{ at } y = H, \tag{12b}$$

$$\psi = q \text{ at } y = H, \tag{12c}$$

$$\psi = q_1^* \text{ at } y = H_1, \tag{12d}$$

$$\psi = q_2^* \text{ at } y = H_2 . \tag{12e}$$

The solution of Eq. (10) subject to the boundary conditions in Eqs.12 (a-e) in terms of stream function is obtained as:

$$\psi = (U_{HS}-1)y - \left((U_{HS}-1)H - q\right)\frac{\int_0^y F(y)dy}{\int_0^H F(y)dy}\ , \tag{13}$$

where , $F(y) = \int_y^H \frac{s}{\mu} ds$.

Solving the above integrations, the *stream functions* in the core, intermediate and peripheral layers are obtained as:

Core region ($0 \le y \le H_1$),

$$\psi = (U_{HS}-1)y - \left((U_{HS}-1)H - q\right)\frac{1}{2}y\frac{\left[3\left(1-\frac{1}{\mu_1}\right)H_1^{\,2} + 3\left(\frac{1}{\mu_1}-\frac{1}{\mu_2}\right)H_2^{\,2} + \frac{3H^2}{\mu_2} - y^2\right]}{\left(1-\frac{1}{\mu_1}\right)H_1^{\,3} + \left(\frac{1}{\mu_1}-\frac{1}{\mu_2}\right)H_2^{\,3} + \frac{H^3}{\mu_2}}, \tag{14a}$$

Intermediate region ($H_1 \le y \le H_2$),

$$\psi = (U_{HS}-1)y - \left((U_{HS}-1)H - q\right)\frac{\left(1-\frac{1}{\mu_1}\right)H_1^{\,3} + \frac{1}{2}y\left[3\left(\frac{1}{\mu_1}-\frac{1}{\mu_2}\right)H_2^{\,2} + \frac{3H^2}{\mu_2} - \frac{y^2}{\mu_1}\right]}{\left(1-\frac{1}{\mu_1}\right)H_1^{\,3} + \left(\frac{1}{\mu_1}-\frac{1}{\mu_2}\right)H_2^{\,3} + \frac{H^3}{\mu_2}}, \tag{14b}$$

Peripheral region ($H_2 \le y \le H$),

$$\psi = (U_{HS}-1)y - \left((U_{HS}-1)H - q\right)\frac{\left(1-\frac{1}{\mu_1}\right)H_1^{\,3} + \left(\frac{1}{\mu_1}-\frac{1}{\mu_2}\right)H_2^{\,3} + \frac{1}{2}y\left(\frac{3H^2}{\mu_2} - \frac{y^2}{\mu_2}\right)}{\left(1-\frac{1}{\mu_1}\right)H_1^{\,3} + \left(\frac{1}{\mu_1}-\frac{1}{\mu_2}\right)H_2^{\,3} + \frac{H^3}{\mu_2}}. \tag{14c}$$

3. FLUID–FLUID INTERFACE ANALYSIS

In the three-layered flow, there are two interfaces. The first exists between the core region and intermediate region. The second interface exists between the intermediate region and peripheral region. The advantage of the present model is that the viscosity of fluids at the interfaces is equal. Using the boundary conditions (12a-e), the algebraic system of equations for the interfaces emerges as:

$$\left.\begin{aligned} A_1 H_1^{\,4} + B_1 H_1^{\,3} + C_1(H_2) H_1 + D_1(H_2) = 0 \\ A_2 H_2^{\,4} + B_2 H_2^{\,3} + C_2(H_1) H_2 + D_2(H_1) = 0 \end{aligned}\right\}, \tag{15}$$

where,

$$A_1 = (U_{HS} - 1)\left(1 - \frac{1}{\mu_1}\right), \tag{16a}$$

$$B_1 = -q_1\left(1 - \frac{1}{\mu_1}\right) - (U_{HS} - 1)\left(1 - \frac{1}{\mu_1}\right)H + \frac{(U_{HS} - 1)H}{2\mu_1} + q\left(1 - \frac{1}{\mu_1}\right) - \frac{q}{2\mu_1}, \tag{16b}$$

$$C_1(H_2) = (U_{HS} - 1)\left(\frac{1}{\mu_1} - \frac{1}{\mu_2}\right)H_2^{\,3} + \frac{(U_{HS} - 1)H^3}{\mu_2} - \frac{3(U_{HS} - 1)}{2}\left(\frac{1}{\mu_1} - \frac{1}{\mu_2}\right)H_2^{\,2}H - \frac{3(U_{HS} - 1)H^3}{2\mu_2} + \frac{3qH^2}{2\mu_2} + \frac{3}{2}q\left(\frac{1}{\mu_1} - \frac{1}{\mu_2}\right)H_2^{\,2}, \tag{16c}$$

$$D_1(H_2) = -q_1\left(\frac{1}{\mu_1} - \frac{1}{\mu_2}\right)H_2^{\,3} - \frac{q_1 H^3}{\mu_2}, \tag{16d}$$

$$A_2 = (U_{HS} - 1)\left(\frac{1}{\mu_1} - \frac{1}{\mu_2}\right), \tag{16e}$$

$$B_2 = -q_2\left(\frac{1}{\mu_1} - \frac{1}{\mu_2}\right) - (U_{HS} - 1)\left(\frac{1}{\mu_1} - \frac{1}{\mu_2}\right)H + \frac{(U_{HS} - 1)H}{2\mu_2} + q\left(\frac{1}{\mu_1} - \frac{1}{\mu_2}\right) - \frac{q}{2\mu_2}, \tag{16f}$$

$$C_2(H_1) = (U_{HS} - 1)\left(1 - \frac{1}{\mu_1}\right)H_1^{\,3} - \frac{(U_{HS} - 1)H^3}{2\mu_2} + \frac{3qH^2}{2\mu_2}, \tag{16g}$$

$$D_2(H_1) = -q_2\left(1 - \frac{1}{\mu_1}\right)H_1^{\,3} - \frac{q_2 H^3}{\mu_2} - (U_{HS} - 1)\left(1 - \frac{1}{\mu_1}\right)HH_1^{\,3} + q\left(1 - \frac{1}{\mu_1}\right)H_1^{\,3}. \tag{16h}$$

In order to compute the interfaces for different sets of values of viscosity of the fluids in different regions, q_1^* and q_2^* can be evaluated by considering the particular value for H_1 and H_2 at $x = 0$ and they are expressed as:

$$q_1^* = (U_{HS}-1)\alpha + \left[\frac{q-(U_{HS}-1)}{2}\right]\frac{\left(2-\frac{3}{\mu_1}\right)\alpha^3 + 3\left(\frac{1}{\mu_1}-\frac{1}{\mu_2}\right)\alpha\beta^2 + 3\frac{1}{\mu_2}\alpha}{\left(1-\frac{1}{\mu_1}\right)\alpha^3 + \left(\frac{1}{\mu_1}-\frac{1}{\mu_2}\right)\beta^3 + \frac{1}{\mu_2}}, \tag{17a}$$

$$q_2^* = (U_{HS}-1)\beta + \left[\frac{q-(U_{HS}-1)}{2}\right]\frac{2\left(1-\frac{1}{\mu_1}\right)\alpha^3 + \left(\frac{2}{\mu_1}-\frac{3}{\mu_2}\right)\beta^3 + 3\frac{1}{\mu_2}\beta}{\left(1-\frac{1}{\mu_1}\right)\alpha^3 + \left(\frac{1}{\mu_1}-\frac{1}{\mu_2}\right)\beta^3 + \frac{1}{\mu_2}}, \tag{17b}$$

where, $\alpha = H_1(0)$ and $\beta = H_2(0)$.

4. PERISTALTIC PUMPING CHARACTERISTICS

Using Eqns. 14 (a-c) and Eqn. (10), the pressure gradient is obtained as:

$$\frac{\partial p}{\partial x_w} = \frac{3\left((U_{HS}-1)H - q\right)}{\left(1-\frac{1}{\mu_1}\right)H_1^{\,3} + \left(\frac{1}{\mu_1}-\frac{1}{\mu_2}\right)H_2^{\,3} + \frac{H^3}{\mu_2}}. \tag{18}$$

Integrating the Eqn. (18) across one wavelength, the *pressure rise* is obtained as:

$$\Delta p = p(1) - p(0) = 3\left\{(U_{HS}-1)\int_0^1 \frac{G(H_1,H_2)}{H^2}\,dx_w - (\bar{Q}-1)\int_0^1 \frac{G(H_1,H_2)}{H^3}\,dx_w\right\}, \tag{19}$$

where, $G(H_1,H_2) = \left\{\left(1-\frac{1}{\mu_1}\right)\frac{H_1^{\,3}}{H^3} + \left(\frac{H_2}{H}\right)^3\left(\frac{1}{\mu_1}-\frac{1}{\mu_2}\right) + \frac{1}{\mu_2}\right\}^{-1}$.

The maximum time-averaged flow rate can be computed at zero pressure rise and is expressed as:

$$\bar{Q}_0 = 1 + \frac{(U_{HS}-1)\int_0^1 \frac{G(H_1,H_2)dx_w}{H^2}}{\int_0^1 \frac{G(H_1,H_2)dx_w}{H^3}}. \tag{20}$$

The maximum pressure rise is also computed at zero time-averaged flow rate as follows:

$$\Delta p_0 = 3\left\{(U_{HS}-1)\int_0^1 \frac{G(H_1,H_2)dx_w}{H^2} + \int_0^1 \frac{G(H_1,H_2)dx_w}{H^3}\right\}. \tag{21}$$

The hydromechanical efficiency, following Shapiro et al. [42], of peristaltic pumping is the *ratio of the average flow rate per wavelength at which work is done by the moving fluid against a pressure head* and the *average rate at which the walls do work on the fluid*. It is computed as:

$$E = \frac{\bar{Q}\,\Delta p}{\phi(I_1 - \Delta p)}, \tag{22}$$

where, $I_1 = \int_0^1 \frac{\partial p}{\partial x_w}\sin(2\pi x_w)dx_w$.

5. TRAPPING ANALYSIS

Trapping is a phenomenon of peristaltic pumping where the streamlines recirculate (i.e. fluid particles start to move in circulation and axial flow vanishes) under specific combinations of the value of occlusion (obstruction in the channel caused by deforming walls) of the peristaltic wave and time-averaged volume flow rate. Here we determine the range of the trapping limit ($\bar{Q}^- < \bar{Q} < \bar{Q}^+$) in the peripheral layer ($H_2 \le y \le H$) at $\psi = 0$ and $y > 0$. At $\psi = 0$, Eqn. (20) reduces to:

$$y^2 = \frac{\left(1-\frac{1}{\mu_1}\right)H_1^{\,2}\left\{A_{11} - 2(U_{HS}-1)H_1\right\} + \left(\frac{1}{\mu_1}-\frac{1}{\mu_2}\right)H_2^{\,2}\left\{A_{11} - 2(U_{HS}-1)H_2\right\} + \frac{H^2}{\mu_2}\left\{A_{11} - 2(U_{HS}-1)H\right\}}{(U_{HS}-1)H - q}, \tag{23}$$

where, $A_{11} = 3((U_{HS}-1)H - q)$.

It is clear that the denominator of Eqn. (23) attains a maximum value at $x_w = 1/4$ and minimum value at $x_w = 3/4$. The range of time-averaged volume flow rate where trapping may occur is computed as:

$$\bar{Q}^+ = \frac{-C(-2+U_{HS}(\phi-1)-\phi)(\phi-1)^2 - 3A(U_{HS}(1-\phi)+\phi)H_{1\max}^{\,2} + 2A(U_{HS}-1)H_{1\max}^{\,3} - 3B(U_{HS}(1-\phi)+\phi)H_{2\max}^{\,2} + 2B(U_{HS}-1)H_{2\max}^{\,3}}{3(C(1-\phi)^2 + AH_{1\max}^{\,2} + BH_{2\max}^{\,2})}, \tag{24a}$$

$$\bar{Q}^- = \frac{C(1+\phi)^2(2+U_{HS}+(U_{HS}-1)\phi) + 3A(U_{HS}+(U_{HS}-1)\phi)H_{1\min}^{\,2} - 2A(U_{HS}-1)H_{1\min}^{\,3} + BH_{2\min}^{\,2}(3(U_{HS}+(U_{HS}-1)\phi - 2(U_{HS}-1)H_{2\min})}{3(C(1+\phi)^2 + AH_{1\min}^{\,2} + BH_{2\min}^{\,2})}, \tag{24b}$$

.

where, $A=\left(1-\frac{1}{\mu_2}\right)$, $B=\left(\frac{1}{\mu_1}-\frac{1}{\mu_2}\right)$, $C=\left(\frac{1}{\mu_2}\right)$, and $\bar{Q}^- < \bar{Q} < \bar{Q}^+$ and $H_{1\max}, H_{2\max}, H_{1\min}$, and $H_{2\min}$ are the values of interfaces at $x_w = 1/4$ and $x_w = 3/4$ respectively.

6. NUMERICAL RESULTS AND DISCUSSION

Extensive numerical evaluations of the closed-form solutions have been conducted in MATLAB symbolic software to examine the influence of key parameters on the electrokinetic multi-layered peristaltic transport. The solutions are visualized in **figs. 2-17**. Specifically we explore the influence of intermediate layer (μ_1) and peripheral layer viscosities (μ_2) and also Helmholtz-Smoluchowski velocity (U_{HS}) on interface shapes, pressure rise, mechanical efficiency and maximum time averaged flow rate. Also the effects of wave amplitude (ϕ) and Helmholtz-Smoluchowski velocity on streamline distributions in the intermediate layer and peripheral layer are studied.

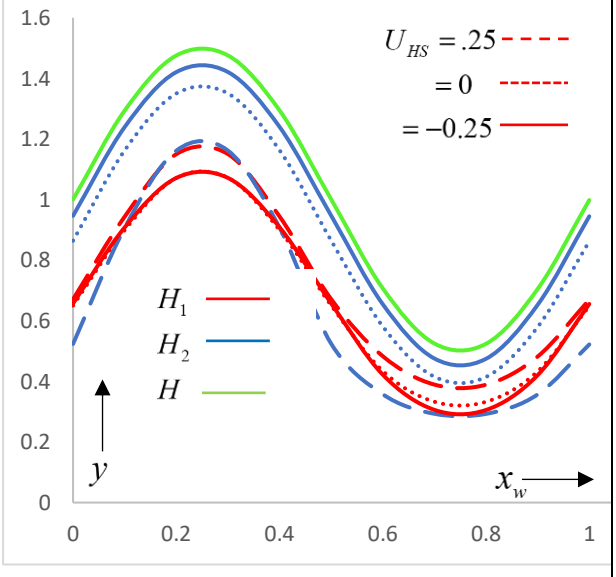

Fig.2 The variation of the shape of the interfaces H_1, H_2 with the value of viscosity $\mu_1 = 10,\ \mu_2 = 0.1$ at $\bar{Q} = 0.1, \alpha = 0.65,\ \beta = 0.85, \phi = 0.5$ for different values of Helmholtz-Smoluchowski velocity.

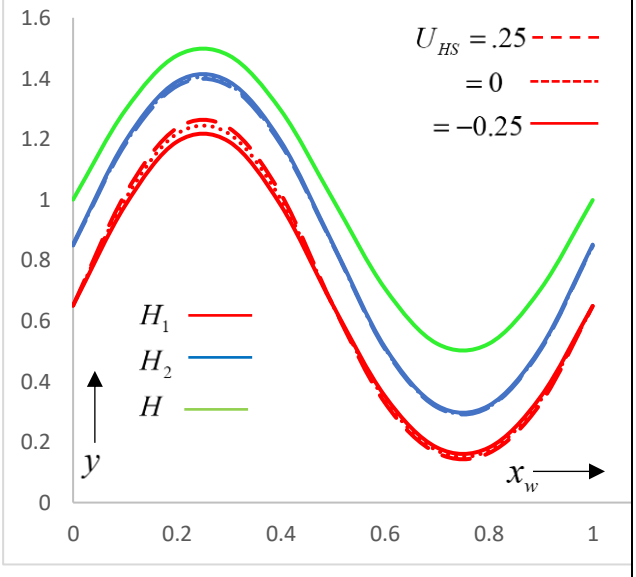

Fig.3 The variation of the shape of the interfaces H_1, H_2 with the value of viscosity $\mu_1 = 0.1, \mu_2 = 10$ at $\bar{Q} = 0.1, \alpha = 0.65,\ \beta = 0.85, \phi = 0.5$ for different values of Helmholtz-Smoluchowski velocity.

$\mu_1 > \mu_2$	$\mu_1 < \mu_2$
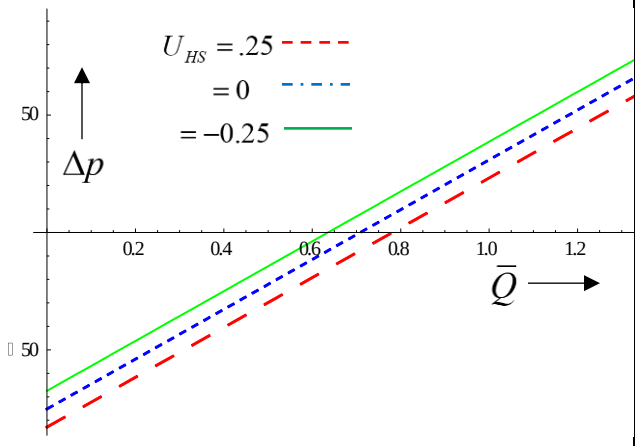	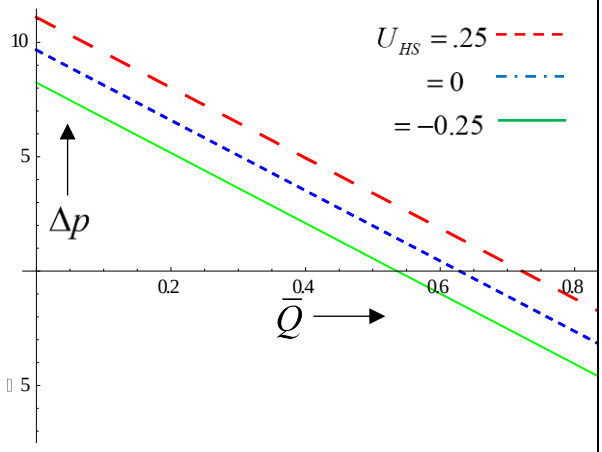
Fig.4 The pressure rise ΔP versus the volume flow rate $\bar{Q}$ with the values of viscosity $\mu_1 = 10, \mu_2 = 0.1$ at $\alpha = 0.65, \beta = 0.85, \phi = 0.7$ for different values of U_{HS}	**Fig.5** The pressure rise ΔP versus the volume floe rate $\bar{Q}$ with the values of viscosity $\mu_1 = 0.1, \mu_2 = 10$ at $\alpha = 0.65, \beta = 0.85, \phi = 0.7$ for different values of U_{HS}
$\mu_1 > \mu_2$	$\mu_1 < \mu_2$
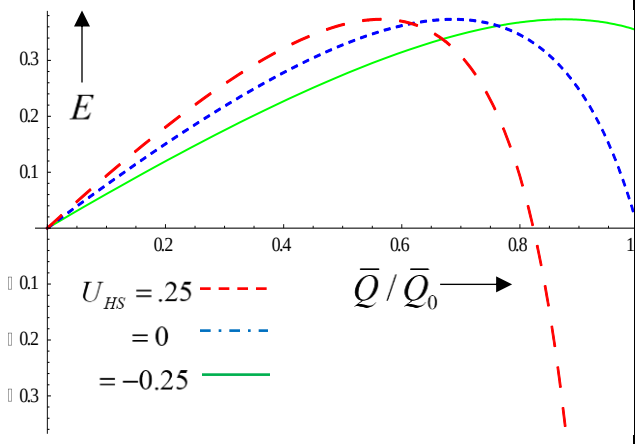	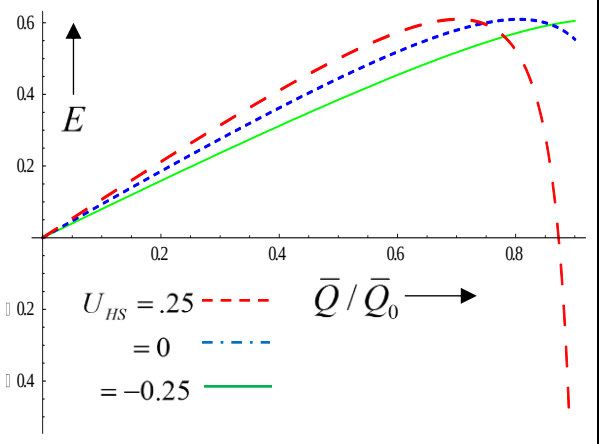
Fig.6 The mechanical efficiency E versus the ratio of the volume rate $\bar{Q} / \bar{Q}_0$ with the values of viscosity $\mu_1 = 10, \mu_2 = 0.1$ at $\alpha = 0.65, \beta = 0.85, \phi = 0.7$ for different values of U_{HS}.	**Fig.7** The mechanical efficiency E versus the ratio of the volume rate $\bar{Q} / \bar{Q}_0$ with the values of viscosity $\mu_1 = 0.1, \mu_2 = 10$ at $\alpha = 0.65, \beta = 0.85, \phi = 0.7$ for different values of U_{HS}.

$\mu_1 > \mu_2$	$\mu_1 < \mu_2$
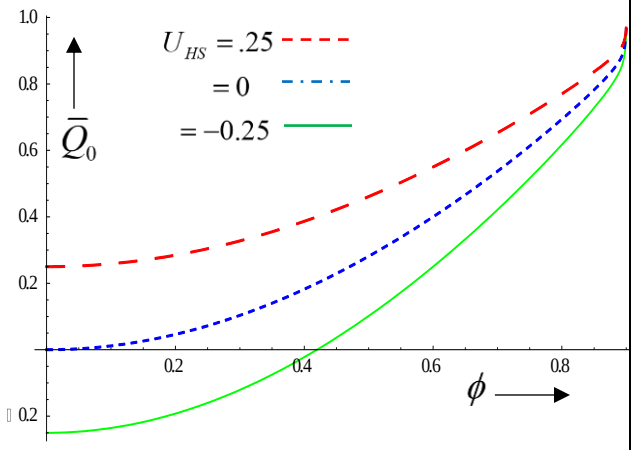	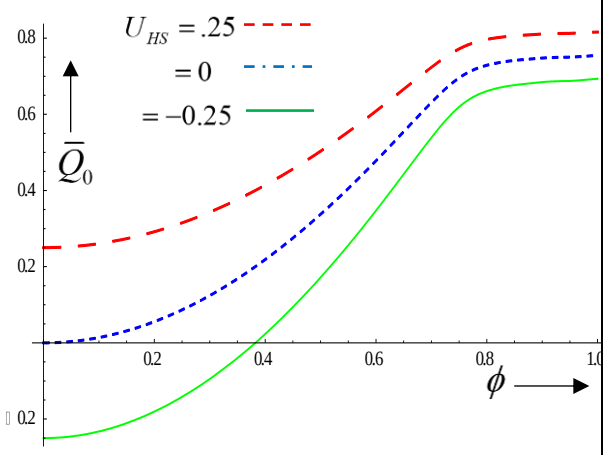
Fig.8 The variation of $\bar{Q}_0$ with ϕ when $\mu_1 = 10, \mu_2 = 0.1$, $\alpha = 0.65, \beta = 0.85$ at different values of U_{HS}.	**Fig.9** The variation of $\bar{Q}_0$ with ϕ when $\mu_1 = 0.1, \mu_2 = 10$, $\alpha = 0.65, \beta = 0.85$ at different values of U_{HS}.

$\mu_1 > \mu_2$	$\mu_1 < \mu_2$
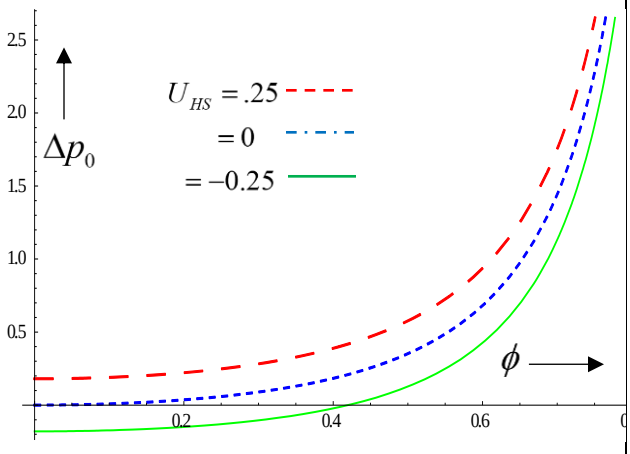	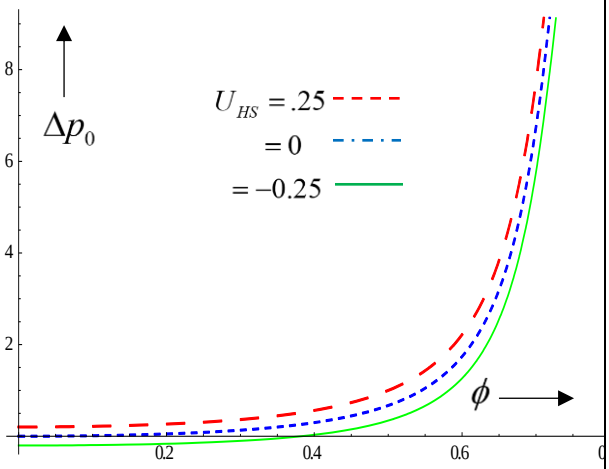
Fig.10 The variation of ΔP_0 with ϕ when $\mu_1 = 10, \mu_2 = 0.1, \alpha = 0.65, \beta = 0.85$ at different values of U_{HS}.	**Fig.11** The variation of ΔP_0 with ϕ when $\mu_1 = 0.1, \mu_2 = 10$, $\alpha = 0.65, \beta = 0.85$ at different values of U_{HS}.

$\mu_1 > \mu_2\ (0 \le y \le H_1)$	$\mu_1 < \mu_2\ \ (0 \le y \le H_1)$
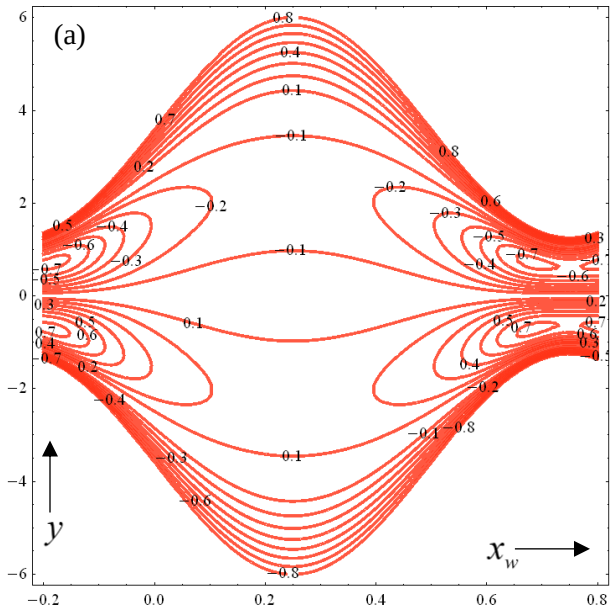	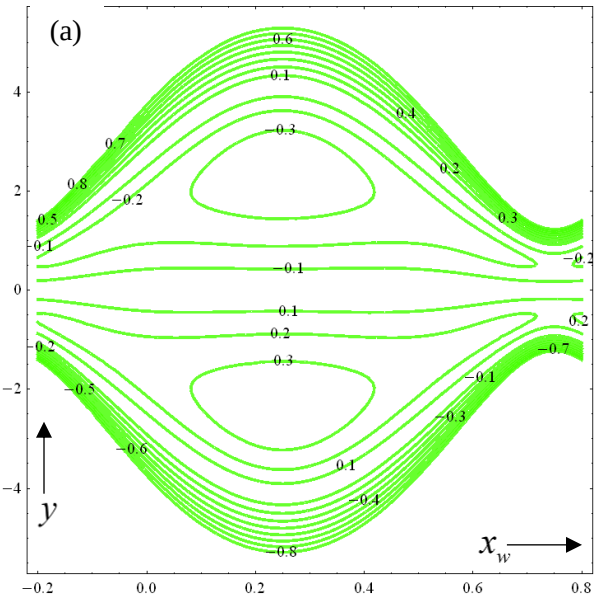
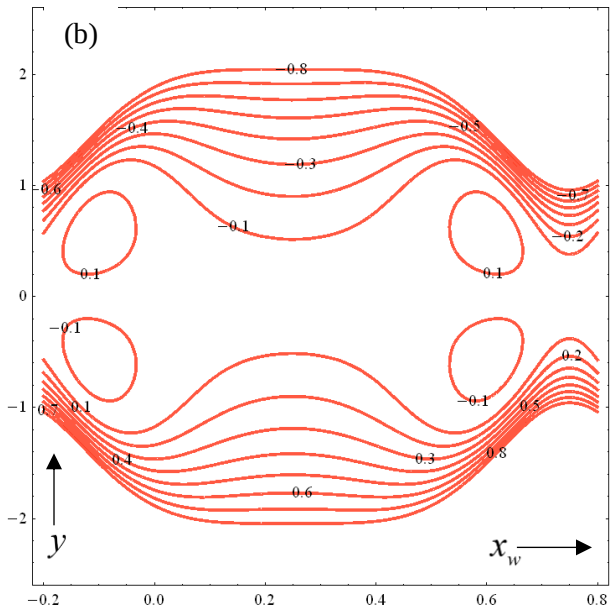	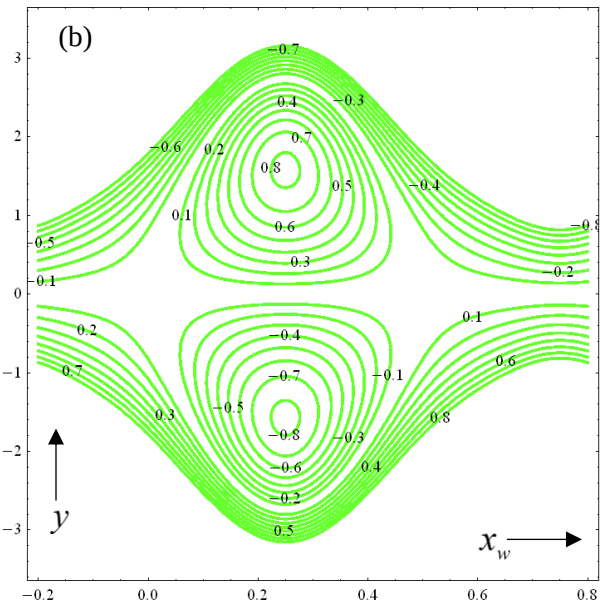

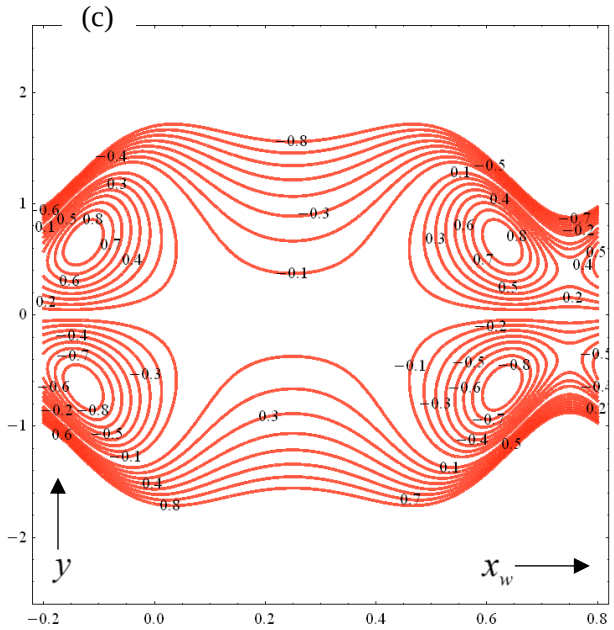

Fig.12 Stream lines in core layer at $\mu_1 = 0.5, \mu_2 = 0.2$, $\phi = 0.7$, $\bar{Q} = 0.8$, $\alpha = 0.65, \beta = 0.85$ (a) $U_{HS} = 1$ (b) $U_{HS} = 0$ (c) $U_{HS} = -1$

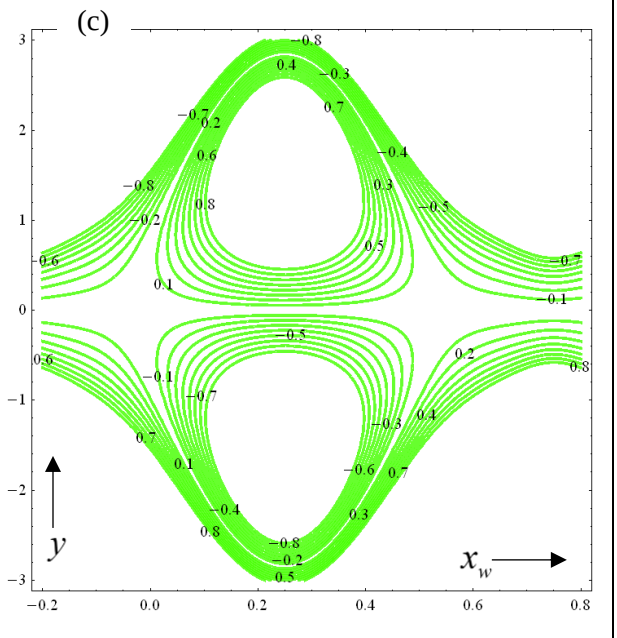

Fig.13 Stream lines in core layer at $\mu_1 = 0.2, \mu_2 = 0.5$, $\phi = 0.7$, $\bar{Q} = 0.8$, $\alpha = 0.65, \beta = 0.85$ (a) $U_{HS} = 1$ (b) $U_{HS} = 0$ (c) $U_{HS} = -1$

$\mu_1 > \mu_2$ $(H_1 \le y \le H_2)$

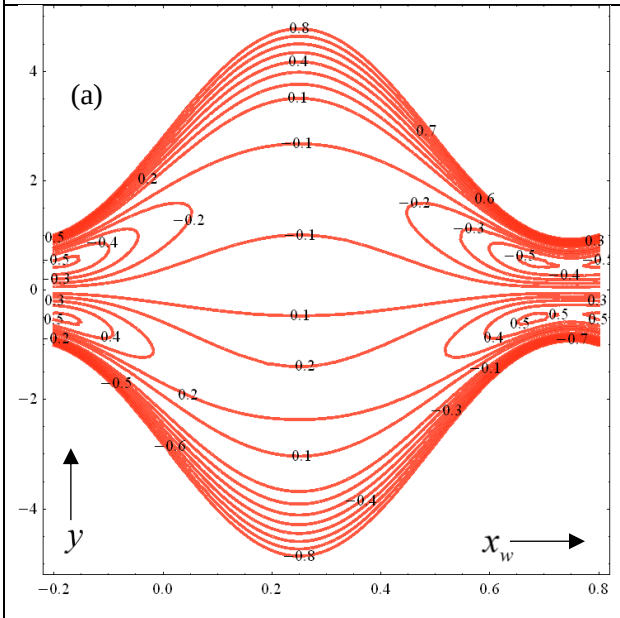

$\mu_1 < \mu_2$ $(H_1 \le y \le H_2)$

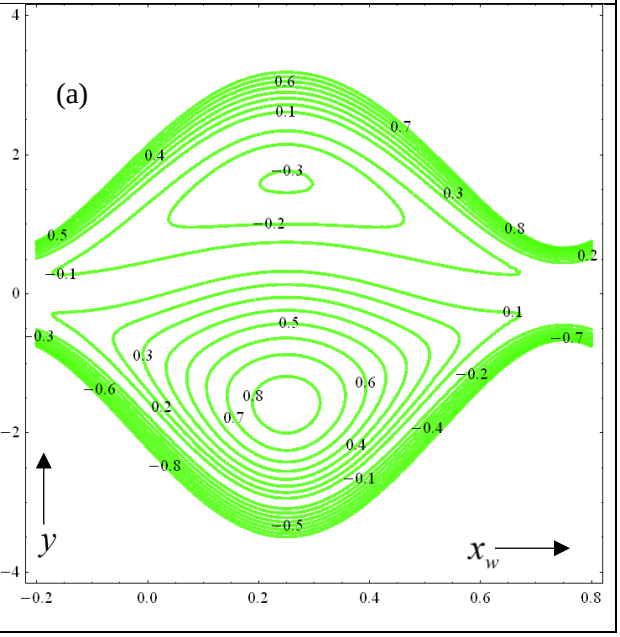

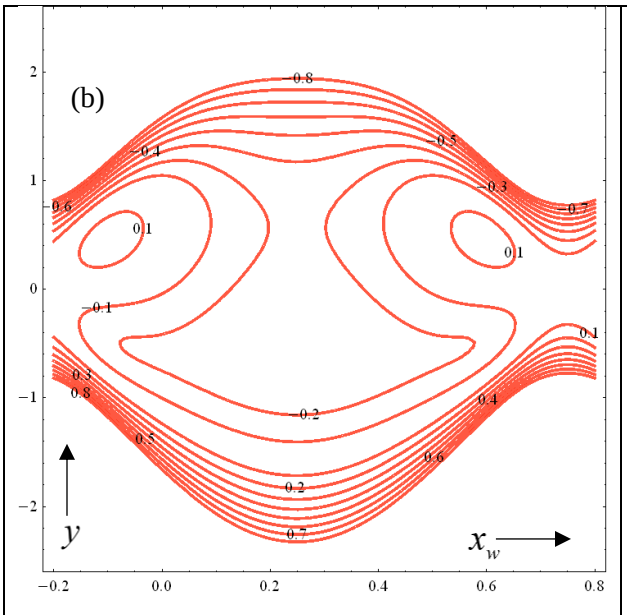

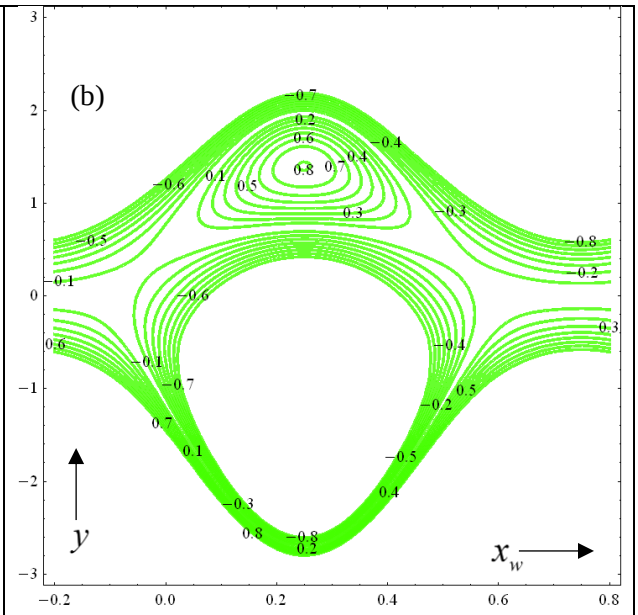

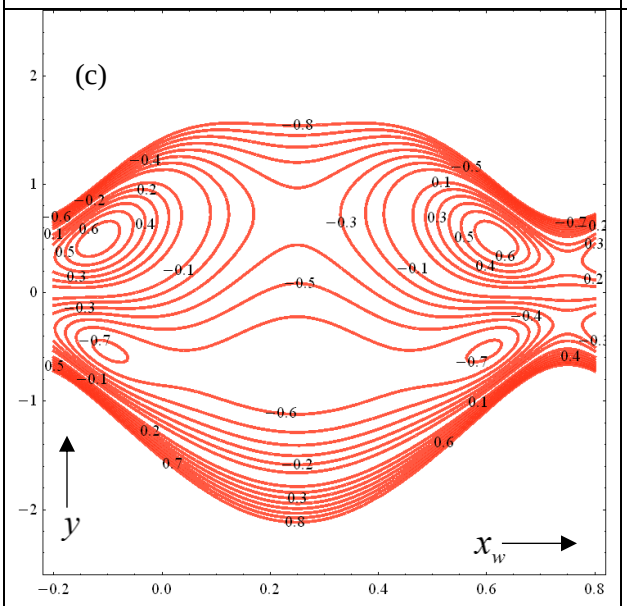

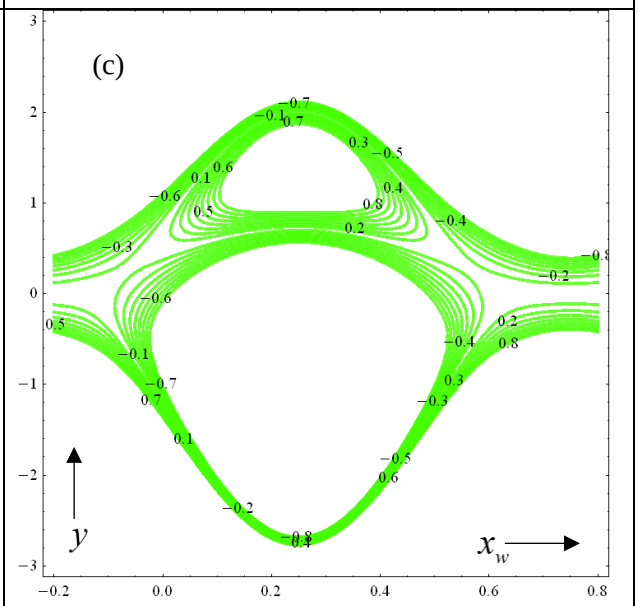

Fig.14 Stream lines in Intermediate layer at $\mu_1 = 0.5, \mu_2 = 0.2, \phi = 0.7,$ $\bar{Q} = 0.8, \alpha = 0.65,$ $\beta = 0.85$ (a) $U_{HS} = 1$ (b) $U_{HS} = 0$ (c) $U_{HS} = -1$

Fig.15 Stream lines in Intermediate layer at $\mu_1 = 0.2, \mu_2 = 0.5,$ $\phi = 0.7,$ $\bar{Q} = 0.8, \alpha = 0.65,$ $\beta = 0.85$ (a) $U_{HS} = 1$ (b) $U_{HS} = 0$ (c) $U_{HS} = -1$

$\mu_1 > \mu_2$ ($H_2 \le y \le H$)	$\mu_1 < \mu_2$ ($H_2 \le y \le H$)
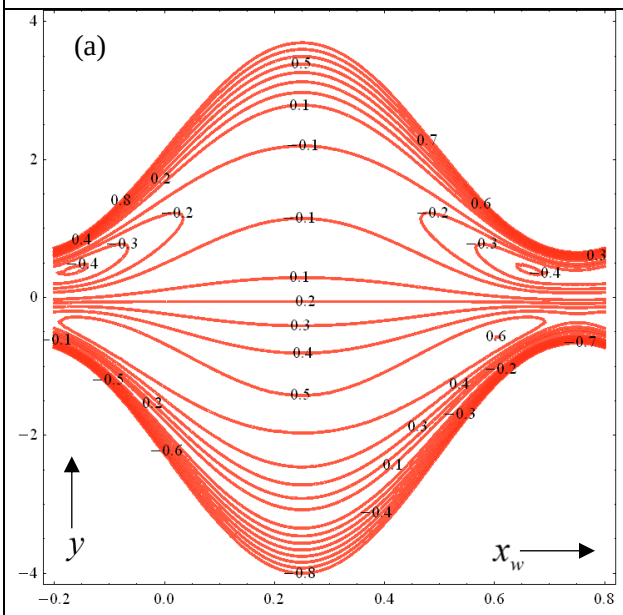	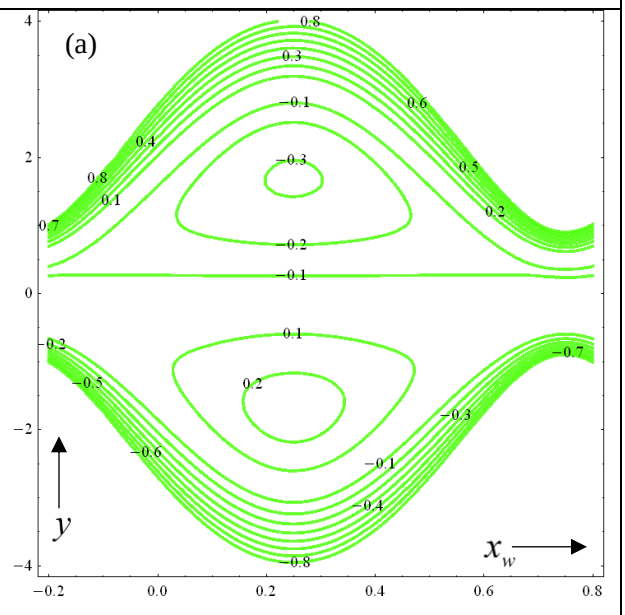
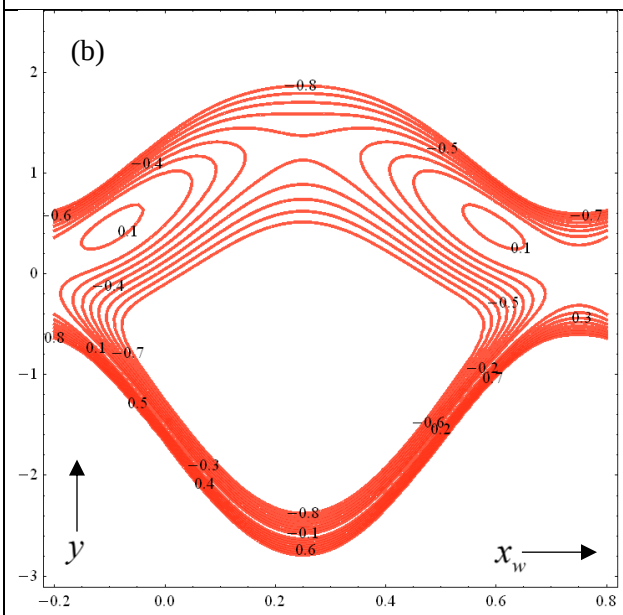	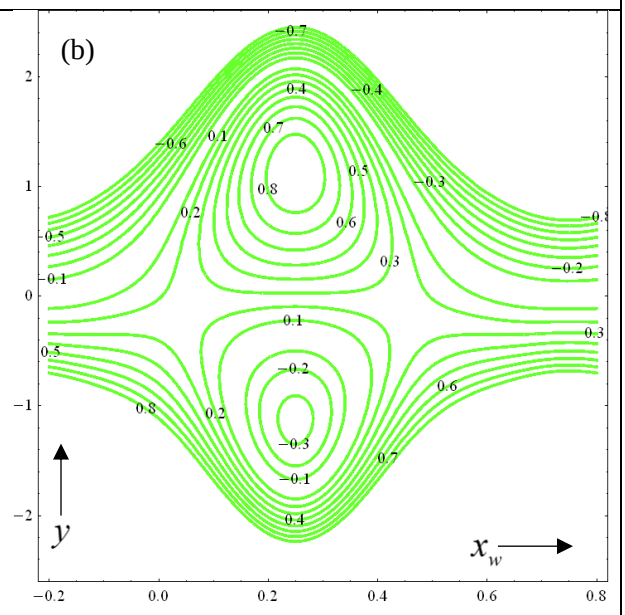

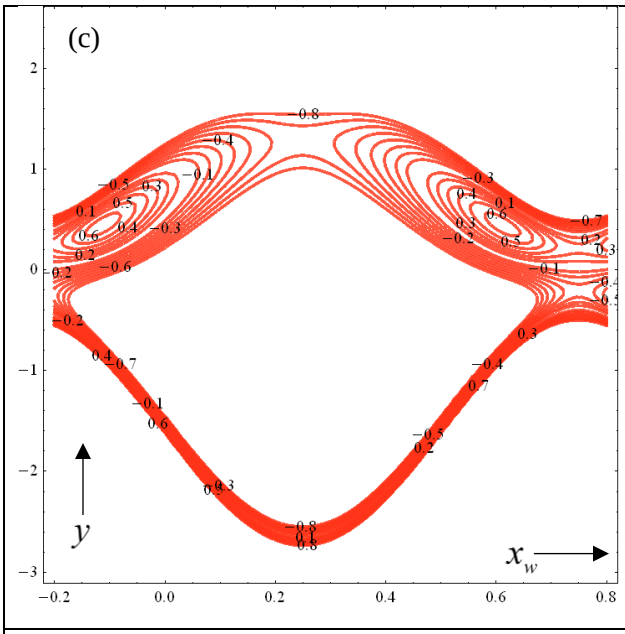

Fig.16 Stream lines in Peripheral layer at $\mu_1 = 0.5, \mu_2 = 0.2$, $\phi = 0.7$, $\bar{Q} = 0.8, \alpha = 0.65$, $\beta = 0.85$ (a) $U_{HS} = 1$ (b) $U_{HS} = 0$ (c) $U_{HS} = -1$

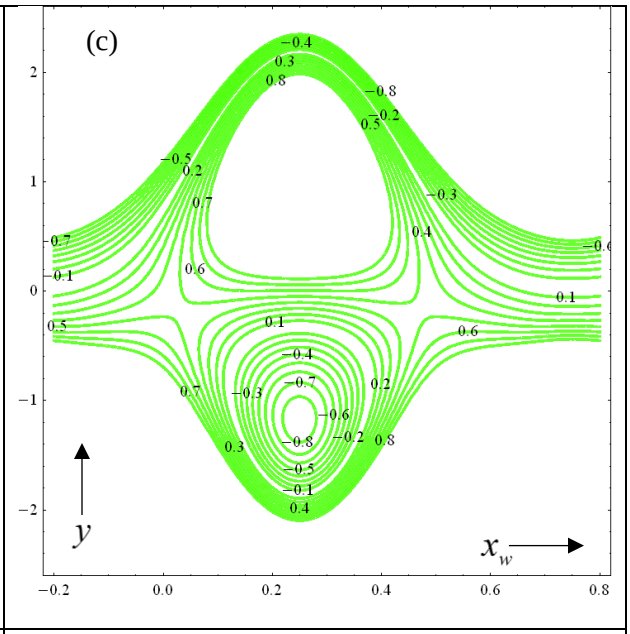

Fig.17 Stream lines in Peripheral layer at $\mu_1 = 0.2, \mu_2 = 0.5$, $\phi = 0.7$, $\bar{Q} = 0.8, \alpha = 0.65$, $\beta = 0.85$ (a) $U_{HS} = 1$ (b) $U_{HS} = 0$ (c) $U_{HS} = -1$

Figs 2-3 illustrate the effects of the Helmholtz-Smoluchowski velocity on interface shapes H_1 and H_2 for two different viscosity ratio scenarios i.e. μ_1 (intermediate) > μ_2 (peripheral) in fig 2 and μ_1 (intermediate) < μ_2 (peripheral) in fig.3. The interface shapes are based on fig.1 i.e. H corresponds to the peripheral layer, H_2 to the intermediate layer and H_1 to the core layer. For fig. 2 the interface shape magnitude is greatest for the peripheral layer, slightly lower for the intermediate layer and significantly lower still for the core layer. With negative Helmholtz-Smoluchowski velocity, there is generally a reduction in H_1 interface shape and an increase in H and H_2 shapes. With positive Helmholtz-Smoluchowski velocity H_2 shape is elevated whereas H_1 is reduced. In the absence of electro-osmotic effect (U_{HS}=0), H_2 is enhanced whereas H_1 is significantly reduced, the latter especially at higher x_w values. For fig 3 wherein the peripheral viscosity exceeds the intermediate viscosity, a similar trend is observed for negative Helmholtz-Smoluchowski velocity although there is less disparity between the H_1 and H_2 plots. For positive negative Helmholtz-Smoluchowski velocity, the H_1 interface profile is maximized. It is also increased for the zero Helmholtz-Smoluchowski velocity case but remains below the positive Helmholtz-Smoluchowski velocity case at lower x_w values, whereas this trend is reversed at higher x_w values. Axial electrical field (E_x) therefore exerts a non-trivial influence on the shape interfaces

for both viscosity scenarios (fig. 2 and fig. 3) since the Helmholtz-Smoluchowski velocity, $U_{HS} = -\frac{E_x \varepsilon z}{\mu c}$, is proportional to E_x.

Figs. 4 and 5 depict the variation in pressure difference as a function of time averaged volumetric flow rate for different values of Helmholtz-Smoluchowski velocity, U_{HS}. In fig. 4 with μ_1 (intermediate layer viscosity) > μ_2 (peripheral layer viscosity), a linear growth in pressure rise accompanies increasing flow rate. With negative Helmholtz-Smoluchowski velocity (maximum electro-osmotic velocity), pressure rise is maximized whereas it is minimized for positive Helmholtz-Smoluchowski velocity. The reverse trends are computed in fig. 5 for which μ_1 (intermediate layer viscosity) < μ_2 (peripheral layer viscosity) i.e. there is a linear decay in pressure rise with increasing flow rate. Positive Helmholtz-Smoluchowski velocity generates the maximum pressure rise and negative Helmholtz-Smoluchowski velocity corresponds to the minimum pressure rise. In both figs. 4 and 5 the zero Helmholtz-Smoluchowski velocity case i.e. vanishing axial electrical field, falls between the other two plots.

Figs. 6 and 7 depict the variation in hydromechanical efficiency (E) as a function of volumetric flow rate ratio, for different values of Helmholtz-Smoluchowski velocity, U_{HS}. Fig. 6 corresponds to μ_1 (intermediate layer viscosity) > μ_2 (peripheral layer viscosity), and fig. 7 to μ_1 (intermediate layer viscosity) < μ_2 (peripheral layer viscosity). In both figures, generally *right-skewed parabolic profiles* are computed for all values of Helmholtz-Smoluchowski velocity. At lower values of volume flow rate ratio, hydromechanical efficiency is *increased* with positive Helmholtz-Smoluchowski velocity (in both figures) and reduced with zero Helmholtz-Smoluchowski velocity and further reduced with negative Helmholtz-Smoluchowski velocity. However with increasing values of volume flow rate ratio, the opposite behavior is computed. Higher magnitudes of hydromechanical efficiency are computed for fig. 7 for all values of flow rate ratio i.e. when μ_1 (intermediate layer viscosity) < μ_2 (peripheral layer viscosity). Greater work is therefore required by the moving fluid relative to the work done by the distending walls when peripheral viscosity exceeds intermediate layer viscosity.

Figs. 8 and 9 illustrate the variation in maximum time-averaged flow rate ($\overline{Q}_o$) as a function of volumetric flow rate ratio, for different values of Helmholtz-Smoluchowski velocity, U_{HS}. Fig. 8 corresponds to μ_1 (intermediate layer viscosity) > μ_2 (peripheral layer viscosity), and fig. 9 to μ_1

(intermediate layer viscosity) < μ_2 (peripheral layer viscosity). Both figures indicate that with increasing peristaltic wave amplitude the maximum time-averaged flow rate grows steadily. However whereas in fig. 8 the profiles tend to converge at high wave amplitude, irrespective of Helmholtz-Smoluchowski velocity, U_{HS}., in fig. 9 there is a more gradual plateau-like effect where profiles become parallel at large wave amplitude. Generally in both figures, positive Helmholtz-Smoluchowski velocity enhances maximum time-averaged flow rate whereas negative Helmholtz-Smoluchowski velocity manifests in a decrease in maximum time-averaged flow rate.

Figs. 10 and 11 present the distributions in maximum pressure rise is also computed at zero time-averaged flow rate (Δp_o) as a function of wave amplitude (ϕ), for different values of Helmholtz-Smoluchowski velocity, U_{HS}. Fig. 10 relates to μ_1 (intermediate layer viscosity) > μ_2 (peripheral layer viscosity), and fig. 11 to μ_1 (intermediate layer viscosity) < μ_2 (peripheral layer viscosity). It is evident from both figures that maximum pressure rise generally increases with increasing peristaltic wave amplitude, in particular at higher amplitudes. Whereas in both figures, positive Helmholtz-Smoluchowski velocity elevates maximum pressure rise, and negative Helmholtz-Smoluchowski velocity induces a reduction in maximum pressure rise, the effect is more prominent in fig. 10 i.e. where peripheral viscosity is lower than intermediate layer viscosity.

Figs 12-17 illustrate the influence of relative values of μ_1 (intermediate layer viscosity) and μ_2 (peripheral layer viscosity), and also Helmholtz-Smoluchowski velocity on streamline distributions in the core layer (figs 12, 13), intermediate layer (figs 14, 15) and peripheral layer (figs. 16, 17). These plots enable the phenomenon of trapping to be examined i.e. the formation of an internally circulating bolus of fluid by closed stream lines. This trapped bolus is pushed along by peristaltic waves. In each set of plots, for example, for the core layer (figs, 12, 13) very different distributions are computed for $\mu_1 > \mu_2$ compared with $\mu_1 < \mu_2$. While symmetry is apparent in both sets of profiles, larger boluses are computed in the case of $\mu_1 < \mu_2$. *B*oluses are also more concentrated in the central zone in this case than they are in the $\mu_1 > \mu_2$ case where they are dispersed towards the outer periphery. Greater concentration of streamlines is computed for negative and positive Helmholtz-Smoluchowski velocity compared with the zero Helmholtz-Smoluchowski velocity case with $\mu_1 > \mu_2$. A greater number of boluses is observed for the case of $\mu_1 > \mu_2$ relative to the $\mu_1 < \mu_2$ case However in the $\mu_1 < \mu_2$ case the bolus magnitudes are substantially larger. There is a progressive intensification in streamline concentrations with a

change in Helmholtz-Smoluchowski velocity from negative, through zero to positive values when the peripheral layer viscosity exceeds the intermediate layer viscosity. For the intermediate layer (figs. 14, 15), a noticeable intensification in the lower half space is observed with increasing Helmholtz-Smoluchowski velocity from negative, through zero to positive values. For the $\mu_1 < \mu_2$ *case*, in particular the lower bolus is *greatly enlargened* with negative Helmholtz-Smoluchowski velocity whereas the upper bolus *shrinks*. In the peripheral layer (figs. 16, 17) there is development of a very large lower bolus for negative Helmholtz-Smoluchowski velocity when $\mu_1 > \mu_2$ whereas the opposite effect is observed for the $\mu_1 < \mu_2$ *i.e. the upper bolus is substantially magnified with* negative Helmholtz-Smoluchowski velocity.

7. CONCLUSIONS

Analytical solutions have been developed for electro-osmotic peristaltic flow in a multi-layered microchannel with axial electrical field effect. The transformed conservation equations have been solved to compute the stream functions in these three layers i.e. core, intermediate and peripheral layers. Interface equations have also been derived. The computations which are relevant to electrokinetic blood flow and micro-channel pumping systems have shown that:

- Negative Helmholtz-Smoluchowski velocity manifests in a decrease in the core layer (H_1) interface shape whereas it causes an increase in peripheral layer *(H)* and intermediate layer (H_2) shapes.
- When intermediate layer viscosity exceeds peripheral layer viscosity there is a linear growth in pressure rise with volumetric flow rate.
- Negative Helmholtz-Smoluchowski velocity (maximum electro-osmotic velocity), enhances pressure rise whereas positive Helmholtz-Smoluchowski velocity decreases it, when intermediate layer viscosity exceeds peripheral layer viscosity. The opposite behavior is observed when intermediate layer viscosity is less than peripheral layer viscosity.
- At lower values of volume flow rate ratio, hydromechanical efficiency is *maximum for* positive Helmholtz-Smoluchowski velocity whether intermediate layer viscosity is less or greater than peripheral layer viscosity.

- With increasing peristaltic wave amplitude and also for positive Helmholtz-Smoluchowski velocity there is an increase in time-averaged flow rate, whether intermediate layer viscosity is less or greater than peripheral layer viscosity.
- Maximum pressure rise is elevated with increasing peristaltic wave amplitude, in particular at higher amplitudes, although higher magnitudes are observed where peripheral viscosity is lower than intermediate layer viscosity.
- In the core layer larger boluses are computed in the case of lower intermediate layer viscosity relative to peripheral layer viscosity although the number of boluses is greater when the intermediate layer viscosity exceeds the peripheral layer viscosity.
- In the intermediate layer, stronger concentration of streamlines is computed in the lower half space with positive Helmholtz-Smoluchowski velocity.
- When intermediate layer viscosity is less than peripheral layer viscosity, the lower bolus is *greatly amplified* with negative Helmholtz-Smoluchowski velocity whereas the upper bolus is reduced.
- In the peripheral layer, a dominant lower bolus is generated for negative Helmholtz-Smoluchowski velocity when intermediate layer viscosity exceeds the peripheral layer viscosity. The converse effect is computed when peripheral layer viscosity exceeds intermediate layer viscosity i.e. *the upper bolus is much larger than the lower bolus* for negative Helmholtz-Smoluchowski velocity.

This study provides exact solutions of a specialized, normalized boundary-value problem of relevance to electro-kinetic hemodynamics and microfluidics. As such the present work is infact a basis for validating for more complex numerical simulations. Although we have inspected the literature this is the first study that considers all the effects reported herein. It is therefore not possible to perform a comparison with published literature since there is none so far with which to provide such a comparison. The trends are however consistent with standard peristaltic (albeit non-electrical) studies and sensible behaviour of the impacting parameters is identified. In the future we hope to generalize the study to use computational fluid dynamics ourselves (e.g. ANSYS FLUENT) but this is not the premise of the current article. The authors of this work have focused on mathematical modelling and theoretical fluid dynamics applications in medicine, not clinical studies since access to such laboratories is not available. However, we envisage that in the future possible links with medical research teams at the Salford General Hospital could be established to

explore clinical implications of the modelling. Furthermore, in the present study we considered *multi-layered variable viscosity* flows in electrokinetic pumping in micro-channels. Blood is known to have *micro-structural rheological characteristics* in narrow vessels and furthermore is *heat-conducting*. These important aspects have been considered by other researchers [43, 44] and will also be explored in future simulations.

REFERENCES

1. M. Liu and J. Yang, Electrokinetic effect of the endothelial glycocalyx layer on two-phase blood flow in small blood vessels, *Microvascular Research*, **78**, 14–19 (2009).
2. A.R. Minerick, A.E. Ostafin and H.C. Chang, Electrokinetic transport of red blood cells in microcapillaries, *Electrophoresis*, **23** (14): 2165-73 (2002).
3. H. Bockelmann, V. Heuveline and D.P. Barz, Optimization of an electrokinetic mixer for microfluidic applications, *Biomicrofluidics*, **6** (2): 24123-2412318 (2012).
4. X. Xing, M. He, H. Qiu and L. Yobas, Continuous-flow electrokinetic-assisted plasmapheresis by using three-dimensional microelectrodes featuring sidewall undercuts, *Anal. Chem.*, **88** (10), pp 5197–5204 (2016).
5. M.J. Pikal, The role of electroosmotic flow in transdermal ionotophoresis, *Advanced Drug Delivery Reviews*, **46**, 281–305 (2001).
6. Levine, S., Marriott, J. R., Neale, G., and Epstein, N., Theory of electrokinetic flow in fine cylindrical capillaries at high zeta potentials, *J. Colloid and Interface Science*, **52**, 136–149 (1975).
7. S. Ghosal, Lubrication theory for electroosmotic flow in a microfluidic channel of slowly varying cross-section and wall charge, *J. Fluid Mechanics*, **459**, 103–128 (2002).
8. J.C. Misra, S. Chandra, *et al.*, Electroosmotic oscillatory flow of micropolar fluid in microchannels: application to dynamics of blood flow in microfluidic devices, *Appl. Math. Mech*, **35**, 749-766 (2014).
9. T.Z. N. Jubery, Modeling and simulation of electrokinetic manipulation of biological particles *PhD Thesis, School of Mechanical and Materials Engineering, Washington State University, USA* (2012).

10. M.S. Pommer, Zhang, Y. T., Keerthi, N., Chen, D., Thomson, J. A., Meinhart, C. D., and Soh, H. T., Dielectrophoretic separation of platelets from diluted whole blood in microfluidic channels, *Electrophoresis*, **29**(6), 1213-1218 (2008).
11. P. Dutta, A. Beskok and T.C. Warburton, Numerical simulation of mixed electroosmotic/pressure driven microflows, *Numerical Heat Transfer Part A: Applications*, **41**(2), 131-148 (2002).
12. L-M. Fu, R-J. Yang, C-H. Lin, Y-J. Pan and G. B.Lee, Electrokinetically driven micro flow cytometers with integrated fiber optics for on-line cell/particle detection, *Analytica Chimica Acta* **507**, 163-169 (2004).
13. P.K. Wong, Wong, J. T., Deval, J. H., and Ho, C. M., Electrokinetic in micro devices for biotechnology applications, *IEEE/ASME Transactions on Mechatronics*, **9**, 366–376 (2004).
14. W. Jie, Lian, M. and Yang, K., Micropumping of biofluids by alternating current electrothermal effects, *Appl. Phys. Lett*. **90**, 234103 (2007).
15. S. Park, Zhang, Y., Wang, T. H.; *et al.* Continuous dielectrophoretic bacterial separation and concentration from physiological media of high conductivity, *Lab Chip*, 11, 2893–2900 (2011).
16. Y. Kang, S.Y. Tan, C. Yang and X. Huang, Electrokinetic pumping using packed microcapillary, *Sensors and Actuators A: Physical*, 133, 375–382 (2007).
17. H. Yang, H. Jiang, A. Ramos and P. García-Sánchez, AC electrokinetic pumping on symmetric electrode arrays, *Microfluidics and Nanofluidics*, 7, 767 (2009).
18. A. Ramos, Electrohydrodynamic and magneto-hydrodynamic micropumps, In: *Hardt S, Schönfeld F (eds) Microfluidics technologies for miniaturized analysis systems*, Springer, pp 59–116 (2008).
19. P.H. Paul, D.W. Arnold, D.W. Neyer and K.B. Smith, Electrokinetic pump application in micro-total analysis systems mechanical actuation to HPLC**,** *Micro Total Analysis Systems 2000, Proc. μTAS 2000 Symposium, Enschede, The Netherlands, 14–18 May* (2000).
20. Y.C. Fung, *Biomechanics: Motion, Flow, Stress and Growth*, Springer, New York (1990).
21. D.K. Whirlow and W. T. Rouleau, Peristaltic flow of a viscous liquid in a thick-walled elastic tube, *Bull. Math. Biophysics*, **27**, 355–370 (1965).

22. J.K. Grabski, J.A. Kolodziej and M. Mierzwiczak, Application of meshless procedure for the peristaltic flow analysis, *Engineering Analysis with Boundary Elements*, 63, 125–133 (2016).
23. N.P. Khabazi, S.M. Taghavi and K. Sadeghy, Peristaltic flow of Bingham fluids at large Reynolds numbers: A numerical study, *J. Non-Newtonian Fluid Mechanics*, 227, 30-44 (2016).
24. M. Javed, T. Hayat, M. Mustafa and B. Ahmad, Velocity and thermal slip effects on peristaltic motion of Walters-B fluid, *Int. J. Heat and Mass Transfer*, 96, 210–217 (2016).
25. D. Tripathi and O. Anwar Bég, A study of unsteady physiological magneto-fluid flow and heat transfer through a finite length channel by peristaltic pumping, *Proc. Inst Mech Eng Part H- J. Eng. Med.,* **226**: 631–644 (2012).
26. D. Tripathi, S. Bhushan and O. Anwar Bég, Analytical study of electro-osmosis modulated capillary peristaltic hemodynamics, *J. Mechanics in Medicine and Biology*, **17**, 5, 1750052.1-1750052.22 (2017). DOI: 10.1142/S021951941750052X
27. J.B. Shukla, Parihar, R. S. and Rao, B. R. P., Effects of peripheral layer viscosity on peristaltic transport of a bio-fluid, *J. Fluid Mech*., **97**, 225-237 (1980).
28. L.M. Srivastava and V.P. Srivastava, Peristaltic transport of a two-layered model of physiological fluid, *J. Biomech*., **15**, 257-265 (1982).
29. V.P. Srivastava and M. Saxena, A two-fluid model of non-Newtonian blood flow induced by peristaltic waves, *Rheol. Acta*, **34**, 406-414 (1995)
30. E.F. Elshehawey and Z.M. Gharsseldien, Peristaltic transport of three-layered flow with variable viscosity, *Applied Mathematics and Computation*, **153**, 417–432 (2004).
31. S.K. Pandey, M.K. Chaube, D. Tripathi, Peristaltic transport of multilayered power-law fluids with distinct viscosities: A mathematical model for intestinal flows, *J. Theor. Biol*., **278**, 11-19 (2011).
32. J.C. Misra and S.K. Pandey, Peristaltic flow of a multilayered power-law fluid through a cylindrical tube, *Int. J. Eng. Sci,* **39**, 387-402 (2001).
33. J.D. Berry, M.R. Davidson and D.J.E. Harvie, A multiphase electrokinetic flow model for electrolytes with liquid/liquid interfaces, *J. Computational Physics*, **251**, 209-222 (2013).
34. G.R. Cokelet and Meiselman HJ., Blood rheology, *Handbook of Hemorheology and Hemodynamics,* IOS Press, USA (2007).

35. Chakraborty, S. (2006). Augmentation of peristaltic microflows through electro-osmotic mechanisms. *Journal of Physics D: Applied Physics*, *39*(24), 5356.
36. Misra, J. C., Chandra, S., Shit, G. C., & Kundu, P. K. (2014). Electroosmotic oscillatory flow of micropolar fluid in microchannels: application to dynamics of blood flow in microfluidic devices. *Applied Mathematics and Mechanics*, *35*(6), 749-766.
37. Bandopadhyay, A., Tripathi, D., & Chakraborty, S. (2016). Electroosmosis-modulated peristaltic transport in microfluidic channels. *Physics of Fluids* (1994-present), 28(5), 052002.
38. Tripathi, D., Bhushan, S., & Bég, O. Anwar (2016). Transverse Magnetic Field Driven Modification in Unsteady Peristaltic Transport with Electrical Double Layer Effects. *Colloids and Surfaces A: Physicochemical and Engineering Aspects*, 506, 32-39.
39. Tripathi, D., Yadav, A., & Bég, O. Anwar (2016). Electro-kinetically driven peristaltic transport of viscoelastic physiological fluids through a finite length capillary: mathematical modelling. *Mathematical Biosciences*, 283, 155-168.
40. Tripathi, D., Bushan, S., & Bég, O. Anwar (2017). Analytical study of electro-osmosis modulated capillary peristaltic hemodynamics. *Journal of Mechanics in Medicine and Biology*, **17**, 1750052 [22 pages].
41. Goswami, P., Chakraborty, J., Bandopadhyay, A. & Chakraborty, S. (2016). Electrokinetically modulated peristaltic transport of power-law fluids. *Microvascular Research*, 103, 41-54.
42. A.H. Shapiro, M.Y. Jaffrin and S.L. Weinberg (1969). Peristaltic pumping with long wavelengths at low Reynolds number, *J. Fluid Mech*., **37**:799–825 (1969).
43. R. Ellahi, M. M. Bhatti, C. Fetecau and K. Vafai (2016), Peristaltic flow of couple stress fluid in a non-uniform rectangular duct having compliant walls, *Communications in Theoretical Physics*, 65(1) 66–72.
44. M.M.Bhatti, A.Zeeshan, R.Ellahi, N.Ijaz (2017). Heat and mass transfer of two-phase flow with electric double layer effects induced due to peristaltic propulsion in the presence of transverse magnetic field, *Journal of Molecular Liquids*, 230, 237–246